Biomaterials 32 (2011) 8234–8242

Contents lists available at ScienceDirect

Biomaterials

journal homepage: www.elsevier.com/locate/biomaterials

Three reversible and controllable discrete steps of channel gating of a viral DNA packaging motor

Jia Geng, Huaming Fang, Farzin Haque, Le Zhang, Peixuan Guo*

Nanobiomedical Center, SEEBME, College of Engineering and Applied Sciences, University of Cincinnati, Cincinnati, OH 45267, USA

ARTICLE INFO

Article history:
Received 28 June 2011
Accepted 11 July 2011
Available online 31 July 2011

Keywords:
Nanotechnology
Bionanotechnology
DNA packaging
Viral motor
Nanopore
Single-molecule sensing

ABSTRACT

The channel of the viral DNA packaging motor allows dsDNA to enter the protein procapsid shell during maturation and to exit during infection. We recently showed that the bacteriophage phi29 DNA packaging motor exercises a one-way traffic property using a channel as a valve for dsDNA translocation. This raises a question of how dsDNA is ejected during infection if the channel only allows the dsDNA to travel inward. We proposed that DNA forward or reverse travel is controlled by conformational changes of the channel. Here we reported our direct observation that the channel indeed exercises conformational changes by single channel recording at a single-molecule level. The changes were induced by high electrical voltage, or by affinity binding to the C-terminal wider end located within the capsid. Novel enough, the conformational change of the purified connector channel exhibited three discrete gating steps, with a size reduction of 32% for each step. We investigated the role of the terminal and internal loop of the channel in gating by different mutants. The step-wise conformational change of the channel was also reversible and controllable, making it an ideal nano-valve for constructing a nanomachine with potential applications in nanobiotechnology and nanomedicine.

1. Introduction

Linear double-stranded DNA viruses package their genomic DNA into a preformed protein shell called the procapsid [1,2]. This DNA encapsulation task is an intriguing step of the viral replication cycle, accomplished by nanomotors using ATP as energy [3–7]. The ingenious design of viral DNA packaging motors and the novel mechanism of action has provoked a broad range of interest among scientists in virology, molecular biology, structure biology, nanotechnology, biophysics, biomaterials, nanomedicine, RNA biochemistry, and therapeutics. In bacteriophage phi29, the nanomotor consists of a protein channel, DNA packaging ATPase gp16, and a ring composed of six pRNA (packaging RNA [8]) to gear the motor [8–10] using one ATP to package 2 [3] or 2.5 [11] base pairs of DNA. The protein hub of this motor is a truncated cone shaped connector [12–14], which contains a 3.6 nm wide central channel that allows the 19.3 kb dsDNA genome to enter during maturation and to exit during the infection process (Fig. 1A–C). The defined phi29 DNA packaging motor, constructed 24 years ago [15], is one of the strongest biomotors [16] assembled *in vitro*. Elucidation of the mechanism of motor action will impact areas of biology, engineering, medicine, and various other nanotechnological fields. The novelty and ingenious design of such machines have inspired the development of biomimetics. *In vitro*, the biomimetic motor could be integrated into synthetic nanodevices [17–21]. *In vivo*, the artificial nanomotors could be used to load drugs, deliver DNA/RNA, pump ions, transport cargos, or drive the motion of components in the heart, eye or other sensing organs in the body. Although the protein sequence of each subunit of the connector holds little sequence homology, and each subunit varies in size [14,22–24], the connector of many viruses displays significant morphological similarity [25]. The structure of the phi29 connector has been previously solved by X-ray crystallography [13,14,26], which shows that it is composed of twelve protein subunits which form a ring with a wider end of 13.8 nm outer diameter buried within the viral procapsid and an extruding narrow end of 6.6 nm. The central channel is 6.0 nm at the wider end and 3.6 nm at the narrow end (Fig. 1C).

Many phenomena concerning procapsid expansion during the life cycle related to DNA packaging of bacteriophage have been reported [27–34]. DNA packaging significantly involves the connector. It has also been reported that the connector is a vital component in the regulation of procapsid shape and size [35,36].

* Corresponding author. Vontz Center for Molecular Studies, ML#0508, 3125 Eden Avenue, Room 2308, University of Cincinnati, Cincinnati, OH 45267, USA. Tel.: +1 513 558 0041; fax: +1 513 558 0024.
E-mail addresses: guop@purdue.edu, guopn@ucmail.uc.edu (P. Guo).

0142-9612/$ – see front matter © 2011 Elsevier Ltd. All rights reserved.
doi:10.1016/j.biomaterials.2011.07.034

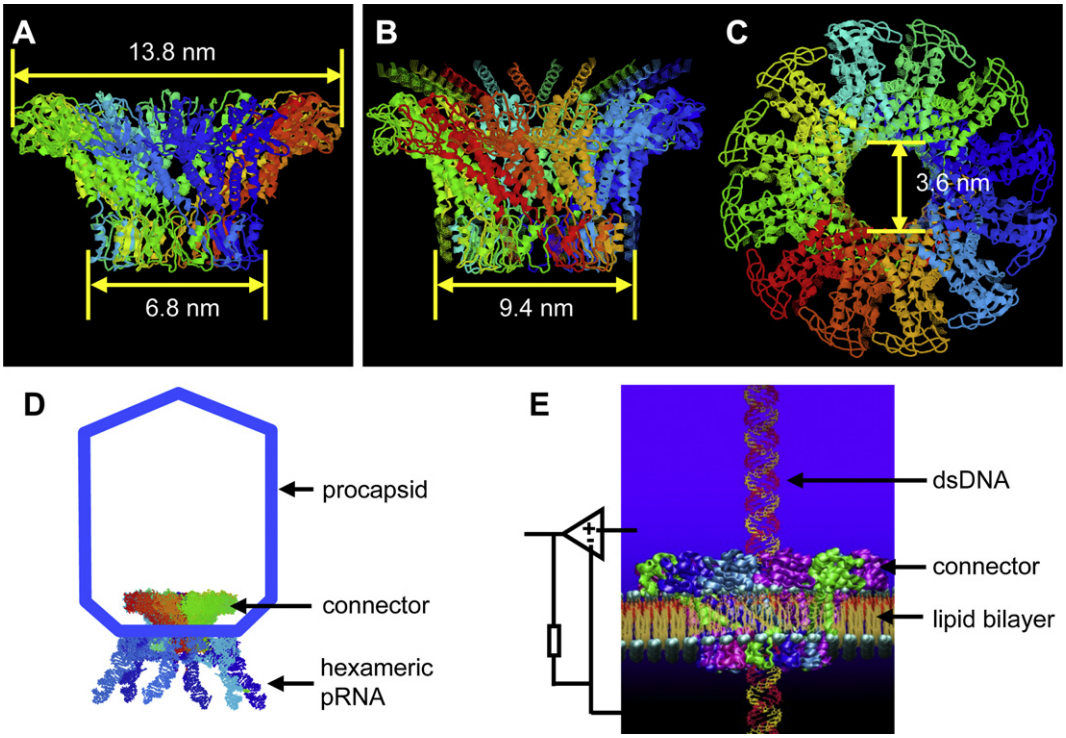

Fig. 1. Illustration of the phi29 connector channel structure. (A) Side view without showing the C- and N-terminal fragment [14]; (B) Side view and (C) bottom view with complete protein sequence [51]; (D) Model of phi29 DNA packaging motor within the procapsid; (E) Illustration of dsDNA translocation through a connector channel reconstituted in an artificial lipid bilayer for the measurement of conductance.

Based on logical analysis, it is reasonable to believe that procapsid expansion is linked to the connector conformational change. However, direct evidence of a conformational change of the connector has never been reported.

We have recently inserted the reengineered connector into a lipid bilayer [20,37] (Fig. 1E). The translocations of ions and dsDNA through the channel demonstrate the potential to use the connector for DNA sensing and fingerprinting at the single-molecule level. We also demonstrated that the phi29 motor channel serves as a valve and exercises a one-way dsDNA traffic mechanism [38]. The direction of DNA trafficking is from the N-terminal narrower end to the C-terminal wider end. This raises a question of how dsDNA is ejected during infection if the channel only allows dsDNA to travel one way. It has been proposed that the motor connector adopts a conformational change after DNA packaging is completed [29]. Such a conformational change renders the channel to allow the dsDNA to come out of the viral procapsid. Here we report that the connector channel indeed exercises conformational change during gating or motor function stimulated by a variety of factors. The conformational change exhibited three discrete identical steps, with each step reducing the size of the channel by one third.

Gating phenomenon has been observed in various protein pores or ion channels [39] and plays a key role in regulating ion transportation through a membrane. Ion channels may be classified by the nature of their gating [40], such as voltage-gated [41], ligand-gated [42], stretch-gated [43], or other gating [40]. Voltage-gated ion channels are activated by changes in electrical potential difference near the channel, while the ligand-gated ion channels are opened or closed in response to the binding of a chemical messenger (i.e., a ligand). There is also recent progress on synthetic channels, which are sensitive to the environmental stimuli, such as temperature [44], voltage [45], pH [46,47], or their combination [48]; but they have a gating mechanism different from protein channels. Here we report a real-time direct observation of the gating of the phi29 DNA packaging nanomotor connector protein channel. It is also interesting to find that this viral protein channel gating can be induced by both voltage and ligand binding, which is similar to the other ion channels.

2. Materials and methods

2.1. Materials

The phospholipid, 1,2-diphytanoyl-sn-glycerol-3-phosphocholine (DPhPC) (Avanti Polar Lipids, Alabaster, AL), Nickel-NTA nanogold (1.8 nm; Nanoprobes), n-decane (Fisher), chloroform (TEDIA) were used as instructed by the vendor. All other reagents were from Sigma, if not specified. The construction and purification of phi29 C-terminal tagged connectors have been reported previously [20,49].

2.2. Regineering, expression and purification of phi29 connector

The construction of the plasmid harboring the gene coding for gp10, the over-expression of gp10 and the purification of phi29 connector have been reported recently [50,51]. The deletion of the tunnel loop (N229–N246) of gp10 was performed by two-step PCR. First, primer pair F1–R1 and primer pair F2–R2 were used to amplify the DNA sequence coding for gp10 (1–228) region and gp10 (247–309) respectively. In the second round of PCR, F1 and R2 were used as primer pairs to link and amplify the PCR product in the first round. The second PCR product was digested with NdeI/XhoI and ligated into NdeI/XhoI sites of the vector pET-21 a(+) (Novagen). The deletion of the N-terminal (1–14) of gp10 was performed by PCR. The sequence coding for gp10 (15–309) region was amplified by a pair of primers. The forward primer contained NdeI restriction site; the reverse primer contained XhoI restriction site and a 6-histidine affinity tag. The PCR product was digested with NdeI/XhoI and ligated into NdeI/XhoI sites of the vector pET-21 a(+) (Novagen).

The connector mutants constructed were expressed, and then were purified with Nickel affinity chromatography [52]. Cells were resuspended with His Binding Buffer (15% glycerol, 0.5 M NaCl, 5 mM Imidazole, 10 mM ATP, 50 mM Na_2HPO_4–NaH_2PO_4, pH 8.0), and the cleared lysate was loaded onto a His•Bind® Resin Column (Novagen) and washed with His Washing Buffer (50 mM Na_2HPO_4–NaH_2PO_4, 15% glycerol, 0.5 M NaCl, 50 mM Imidazole, 10 mM ATP, pH 8.0). The His-tagged connector was eluted by His Elution Buffer (50 mM Na_2HPO_4–NaH_2PO_4, 15% glycerol, 0.5 M NaCl, 0.5 M Imidazole, 50 mM ATP, pH 8.0).

2.3. Electrophysiological measurements

A bilayer was formed on a thin Teflon film partition (aperture 200 μm in diameter) which separates a bilayer lipid membrane (BLM) chamber into a *cis*- and *trans*-chamber (compartment). The *cis*-chamber refers to the grounded compartment to which the connector-reconstituted liposome is added. Connector channel insertion into the bilayer has been described previously using vesicle fusion [20]. Briefly, connector-reconstituted liposomes were prepared using a dehydration–rehydration method and further extruded to form unilamellar liposomes. The reconstituted liposomes were further diluted by 10-fold using the conducting buffer before applying to BLM chambers. The final concentration of added protein was 5–50 μg/mL.

For electrophysiological measurements, both compartments in the BLM chamber were filled with a conducting buffer (1 M NaCl, 5 mM Tris, pH 7.8, if not specified). A pair of Ag/AgCl electrodes connected directly to both compartments was used to measure the current traces across the bilayer lipid membrane. The current trace was recorded using an Axopatch 200B patch clamp amplifier coupled with the Axon DigiData 1322A analog–digital converter (Axon Instruments) or the BLM workstation (Warner Instruments). All voltages reported were those of the *trans*-compartment. Data was low band-pass filtered at a frequency of 5 kHz or 1 kHz and acquired at a sampling frequency of 10 kHz. The PClamp 9.1 software (Axon Instruments) was used to collect the data, and the software Origin Pro 8.0 was used for data analysis.

2.4. Probing connector conformational change using antibody

C-His connector and rabbit polyclonal antibodies (where) specific for His tag were added to the bottom chamber and measured under a voltage of −75 mV at the bottom chamber (a buffer containing 150 mM NaCl at pH 7.8).

2.5. Probing connector conformational change using Nickel-NTA nanogold

Conductance measurements were carried out under asymmetric ionic conditions [53]. The chamber without nanogold contained 1 M NaCl, 20 mM Tris (pH 7.6). For the chamber that contained nanogold, the NaCl concentration was reduced to 150 mM to avoid the high salt effect that might interfere with the binding of nanogold to the His-tagged connecter. DNA was premixed in both chambers with the conducting buffer. After forming the bilayer, a final concentration of 150 pM Ni-NTA nanogold (1.8 nm; Nanoprobes) was added to the chamber and incubated for 5–10 min to ensure an even particle distribution before the connector-reconstituted liposomes were added to the chamber.

3. Results

3.1. Discrete one-third step-wise conformational change during high-voltage gating

The connector protein embedded in the lipid bilayer was stable and displayed a uniform conductance under a wide range of experimental conditions including different salt concentrations and varying pH [37], and has a uniform conductance in each of the conditions. At a constant holding potential (−75 mV), the channel conductance is uniform (Fig. 2A). However, when a higher potential (−150 mV or +200 mV) was applied, a 3-step channel size reduction was often observed immediately thereafter (Fig. 2C and D), which is very similar to the gating behaviors of membrane proteins. In the given experiment conduction (1 M NaCl with 5 mM Na_2HPO_4 buffer, pH 12), the step size of a single C-His connector is around 190 pA at +75 mV (Fig. 2A), and −190 pA at −75 mV (Fig. 2B). The channel was stable over minutes, and even hours without any blockade or vibration. When the voltage was switched to −150 mV, the current through the channel doubled in accordance with the voltage increase from −190 pA to −380 pA. Immediately after that, the same channel closed after a three-step reduction in 5 s (Fig. 2C). Each reduction step size was 120 pA, accounting for 31% of the entire channel. This 3-step channel gating can be triggered by the high voltage despite the buffer conditions. It is interesting to note that after the 3-step reduction, there was still a residual current of 20 pA opening, equal to ~5.3% of one channel. Similar results were observed at higher potentials of 200 mV (Fig. 2D).

3.2. Reopening of the gated channel by voltage dropping

It was also observed that the gating of the C-His connector protein channel was reversible. When a transmembrane voltage of 0 pA was applied for 10–30 s, the gated channel was observed to reopen (Fig. 3). After the channel shutting down was triggered by higher voltage (−100 mV in Fig. 3A, and −150 mV in Fig. 3B), a lower voltage was applied to allow the connector protein to recover. It was found that the conductance of the channels restored to their original state within 10 s.

3.3. Discrete one-third step-wise conformational change of connector induced by protein binding to the C-terminal

A C-terminal His-tagged connector and rabbit polyclonal antibody (Ab) specific against His tag were used to measure the conductivity under a voltage of −75 mV with the negative pole placed at the bottom chamber (the *-trans* side). Since the channel exercises a one-way traffic mechanism, orientation of the connector was determined by their capability to translocate dsDNAs which was placed in only one, either top or bottom of the two chambers via the polarity of applied electrical current (see Ref. [38] for details). Addition of the Ab to the bottom chamber (Fig. 4B) resulted in six discrete 31% current reduction steps for two connectors, indicating binding events induced by interaction of one Ab molecule with one of the two connector channels. As a negative control, two connectors were inserted into BLM with the His-tagged C-terminal exposed to the bottom chamber. DNA was premixed with conducting buffer before the insertion of the connector channels. When the Ab was added to the top chamber, no binding events were observed (Fig. 4A). The results indicate a three-step conformational change of connector after the anti-His antibody bound to the His tag at the C-terminal.

3.4. Discrete one-third step-wise conformational change of the connector channel induced by Ni-NTA nanogold binding to the C-terminal

A 1.8-nm Ni-NTA nanogold particle was used to bind to the His-tag at the C-terminal of the connector. The binding was promoted via a Ni-NTA/His-tag interaction. The nanogold was premixed with the conducting buffer (asymmetric conditions; see Methods) at only one side of the chamber (the *trans*-side). In the presence of a single or multiple connector channels, the nanogold only bound to a connector with its His-tagged C-terminal end oriented toward the *trans*-chamber to the bottom, and did not bind to connectors with the N-terminal facing the *trans*-side. Clear discrete step-wise closing of the channels with a corresponding decrease in conductance was observed when a single connector with the appropriate orientation for nanogold binding was present (Fig. 4C). Binding of each nanogold particle resulted in ~31% reduction in channel current. Such observations enabled the direct counting of the number of nanogold particles bound to each connector. The step size of each current reduction, resulting from the binding of one nanogold particle, was nearly identical, even in the case of membranes with multiple channels (data not shown).

3.5. Gating behavior of mutant connector with the internal 18-amio acid flexible loop or the N-terminal 14-amino acid removal

Phi29 connector protein contains three flexible fragments, the N-terminal fragment amino acid (aa) 1–14, the internal fragment aa 229–246, and the C-terminal fragment aa 287–309 (Fig. 5A) [13,14]. The structures of these three fragments were not included in the crystal structure due to their flexible nature. The flexibility of

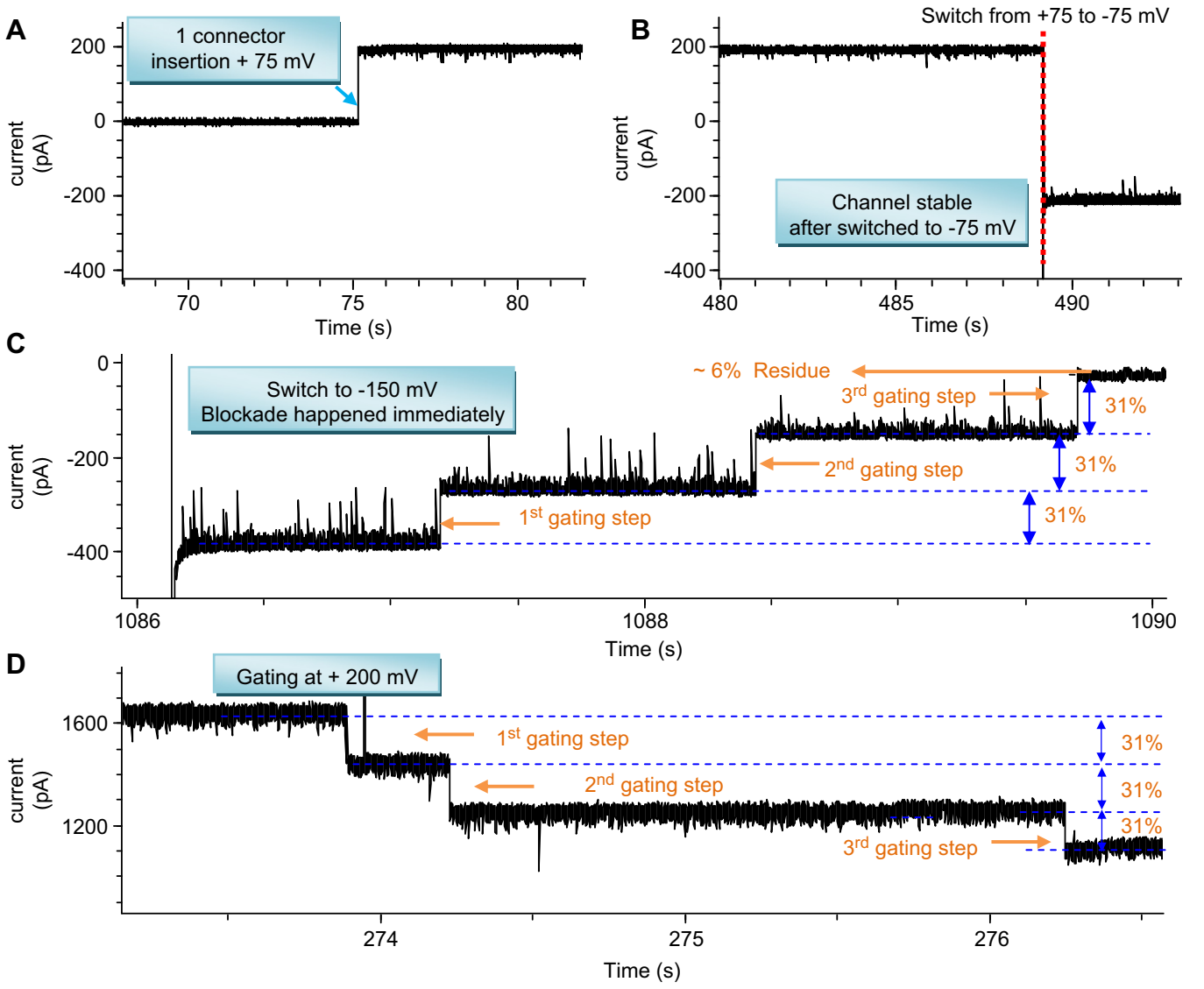

Fig. 2. Step-wise gating of C-His connector channel triggered by high voltage. (A) The channel was stable at +75 mV and (B) at −75 mV after insertion into a bilayer. (C) Immediately after a high voltage (−150 mV) was applied, the channel gated in 3 discrete steps. (D) Similar events happened at +200 mV.

the connector channel is expected to play a critical role in motor motion and DNA translocation, instead of channel structure construction. To investigate whether these three loops were involved in channel gating, three connector mutations, gp10-C-His/NΔ1–14, gp10-C-His/Δ229–246, and gp10-C-Strep/CΔ25 were constructed, with the deletion of the loop aa 1–14, 229–246, and 285–309, respectively (Fig. 5B). The step-wise gating was observed under both the higher holding potentials and a ramping voltage (from −150 mV to +150 mV, or from −200 mV to +200 mV). Fig. 6A and B shows the events happened on a gp10-C-His/NΔ1–14 connector channel, which has a similar channel conductance with the C-His connector. Gating occurred immediately when the ramping began at −150 mV, as shown by the step-wise reductions in the slope of the current trace (Fig. 6B). The slope restored to its original state under −50 mV, indicating that the channel conductance reopened completely. Complete gating happens at a positive potential higher than +110 mV. Such a ramping voltage was applied periodically to test the possibility of the channel gating and reopening (Fig. 6C and E). It was found that both C-His (Fig. 6D) and gp10-C-His/NΔ1–14 can be closed completely after several ramping circles, while the gp10-C-His/Δ229–246 were much less likely to be gated completely (Fig. 6E). The current trace through gp10-C-His/Δ229–246 was still linear (Fig. 6F) under 120 ramping cycles after 3 h, indicating the amazing stability of the channel conductance and significant differences between the channels with/without intact internal loops.

3.6. *The effect of the C-terminal region in regulating the conformational change*

The aforementioned results suggest that phi29 connector implemented a conformational change with three discrete steps. It was proposed that these three steps of conformational change is regulated by the interaction of DNA with the connector, and the binding or contact of components to the C-terminal would result in the similar discrete steps of conformational change. This proposal was supported by a conductance assay using mutant connector conjugated with a His-tag to its C-terminal and incubated with anti-His tag antibody or nanogold coated with Ni-NTA (Fig. 4). It was hypothesized that the translocation of DNA into the procapsid or the internal pressure of the fully packaged DNA within the procapsid might lead to the contact of DNA with the C-terminal

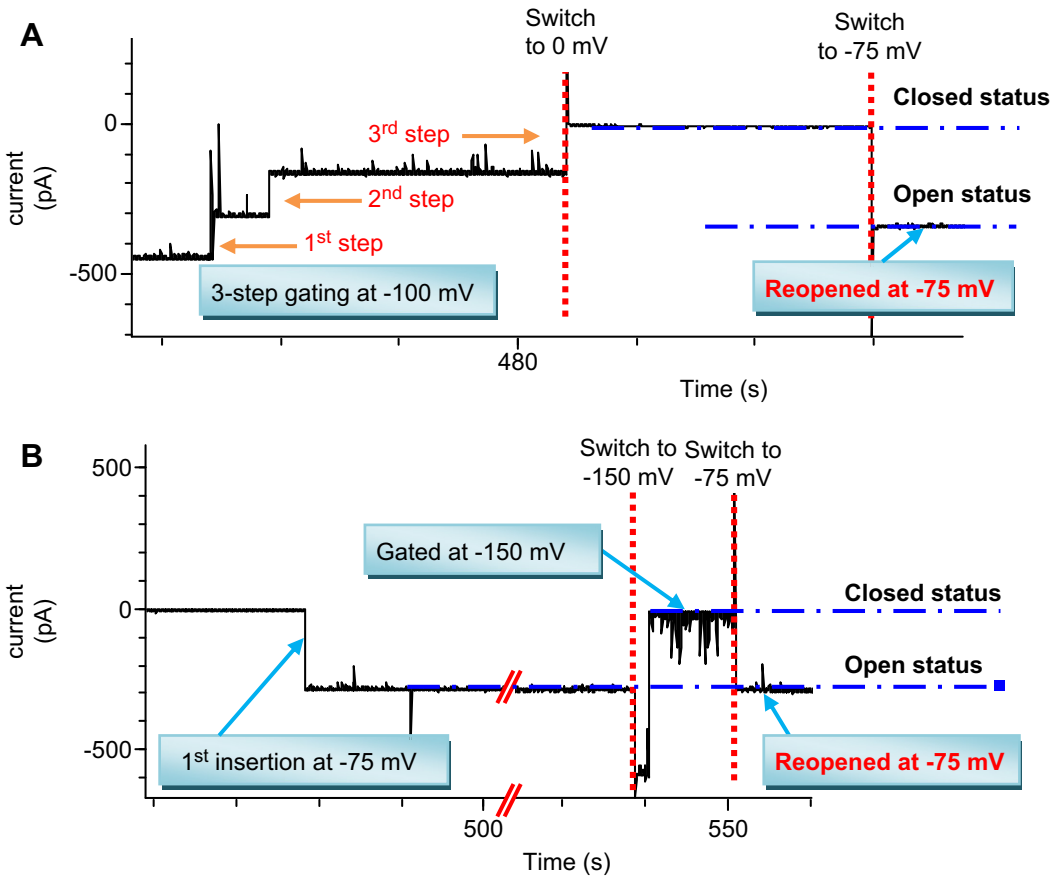

Fig. 3. Controllable and switchable closing and reopening of the connector channel. (A) The C-His channel with three steps of gating at high voltage (−100 mV or −150 mV) was reopened after the voltage was reduced to 0 mV. (B) The channel closed at −150 mV was reopened to its original size at a lower voltage of −75 mV.

flexible domain, inducing a conformational change with two subsequence functions: 1) to prevent the dsDNA from exit; and 2) to prepare a new channel configuration to facilitate the injection of DNA during the host cell infection process. To further confirm this hypothesis, a connector mutant with the removal of a 25-amino acid segment at each C-terminal of the 12 subunits was constructed. Similarly, a strep-tag was conjugated to the C-terminal fused to amino acid #287. Conductance assay of the mutant connector by electrical ramping revealed that three discrete steps of conformational changes were also observed (Fig. 6G). However, the discrete steps of 32% conductance change were not observed in the presence of streptavidin.

4. Discussion

Viral DNA packaging has been investigated extensively in many viral systems, but the actual mechanism remains elusive. During the last several decades, many models have been proposed to interpret the mechanism of motor action. These include 1) Gyrase-driven supercoiled and relaxation [6,54,55]; 2) Force of osmotic pressure [56]; 3) Ratchet mechanism [57]; 4) Brownian motion [58]; 5) Five-fold/six-fold mismatch connector rotating thread [59]; 6) Supercoiled DNA wrapping [60]; 7) Sequential action of motor components [11,61]; 8) Electro-dipole within central channel [14]; and, 9) Connector contraction hypothesis [62]. All these models are very intriguing, however, none have been fully supported by conclusive experimental data. In other cases, various models were validated in one viral system but disproved in another. The five-fold/six-fold mismatch connector rotating thread model [59] has been popular for more than 30 years, since this model could bring about a new mechanical motor prototype. Even within the last several years, numerous laboratories, including our own, have persevered to search, interpret, match, link, and even design a five-fold ring to adapt findings to this fascinating and extraordinary model [11,63–65]. Unfortunately, recent studies in many viral DNA packaging motors reveal that the stoichiometry of motor components is not an odd number but actually an even number [19,66–68]. In 1998, Guo and co-workers first proposed and revealed that the mechanism of DNA packaging is simply via a mechanism similar to the hexameric AAA+ ATPase that translocate dsDNA during DNA replication and repair [9]. The finding of even-number structures is consistent with the mechanism of many other well-studied DNA-tracking motors [69–72] and the AAA+ ATPase family. Most recent publications [52,65,73–75] all support our long-term findings [19,68,76] that pRNA dimer is indeed the building block for hexameric structure [76]. X-ray crystallography also confirmed that pRNA forms a dimer in solution and the dimer forms a tetramer in the absence of the procapsid [65], supporting the theory that the dimer is indeed the building block of the hexamer and the sequential action in hexamer assembly is 2 → 4 → 6. Furthermore, explicit results conclude that the connector does not rotate during the DNA translocation process [77,78]. Recently, Guo and co-workers proposed a “Pushing through a one-way valve model” [2,38]. In this model, the connector remains as non-rotating valve to allow dsDNA travel one way toward the procapsid; DNA translocation is induced by a DNA packaging enzyme or terminase, which pushes a certain length of DNA into the procapsid segment by segment. This model strongly agrees with many recent findings. Most recently, it

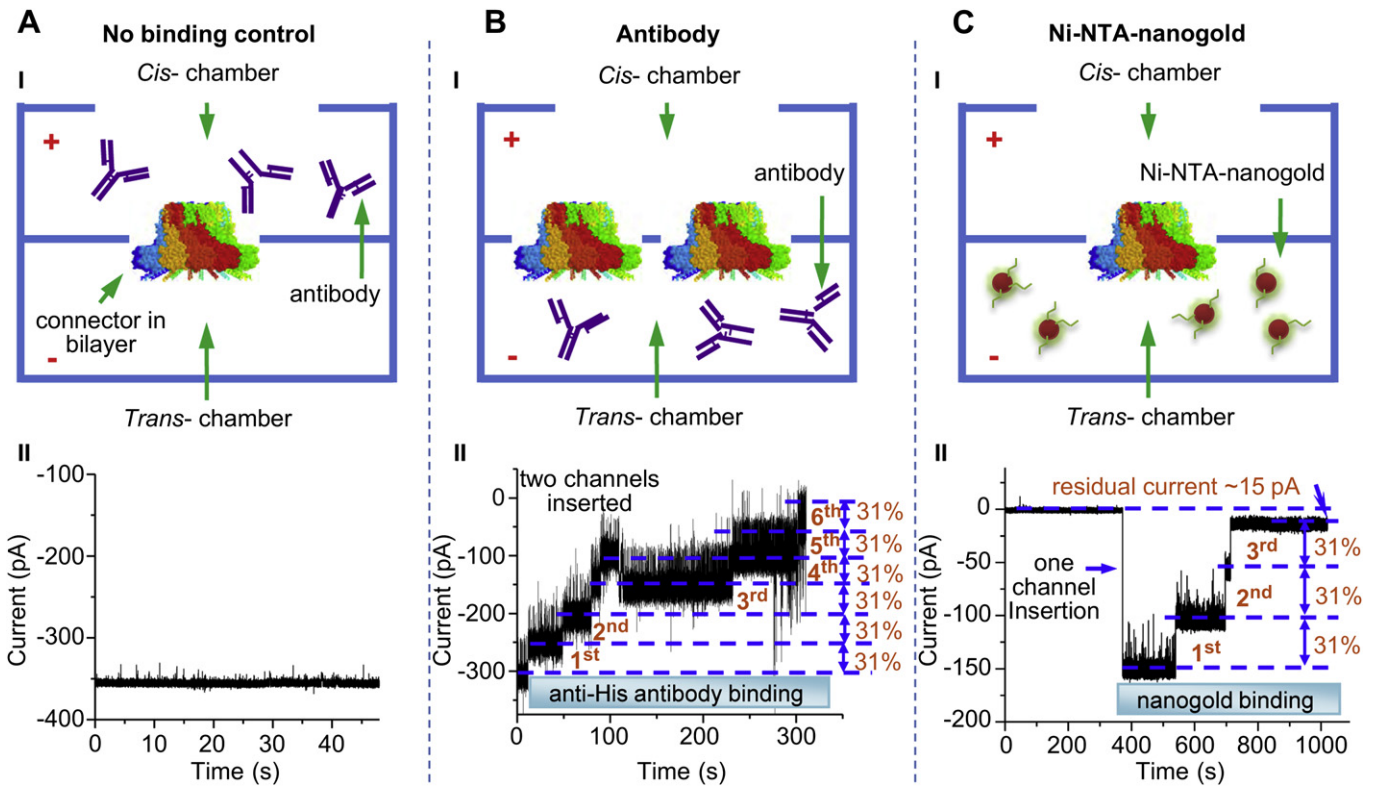

Fig. 4. Changes of channel size by binding to C-terminal. (A) Negative control since the antibody was placed in the *cis*-chamber opposite to the C-terminal. (B) Six discrete steps of changes for two C-His-tagged connector channels induced by anti-His tag antibodies. (C) Three discrete steps of changes for one C-His-tagged connector channels induced by Ni-NTA nanogold binding (1.8 nm).

was reported that under an external electrical force, the channel of the phi29 nanomotor favored DNA entry but blocked DNA departure [38]. The one-way traffic property implies that during the packaging of dsDNA via the active motor, dsDNA travels in only one direction from the narrow external end (N-terminal) toward the wider internal end (C-terminal) of the channel. Essentially, the channel functions as a one-way valve. Thus, these results suggest that dsDNA packaging occurs through the combination of two separate tasks. The first task is the active pushing mechanism [2,38,79,80] provided by the ATPase, gp16, bound to pRNA (the fulcrum) of phi29, actively pushing dsDNA coupled with hydrolysis of ATP. In other dsDNA phage systems, two proteins (terminases) act in combination where the large subunit grips onto the small subunit for use as a fulcrum as with pRNA of phi29. The second task is the control of DNA migration direction with a one-way valve mechanism of the channel [38]. The mechanism providing force through the one-way valve connector also agrees with the finding in T4 phage system by Black and co-workers [79,80]. They found that dsDNA was crunched and the compressed if the DNA entry was blocked at the front end [79,80]. Although the authors interpreted that the force for the crunching and compression is due to torsional force from the coiled DNA at the external end, it is not contradictory to support our finding that the ATPase gp16 functions similar to the DNA-tracking AAA+ family that twisting or rotating the dsDNA [81]. Our new model is also supported by the finding that in the T4 DNA packaging system, both ends of DNA are able to stay outside of the procapsid [79,80]. If the motor would have implemented a pulling instead of pushing function, it would be difficult to interpret how the initiation of DNA translocation begins when both ends are located outside the channel [79,80].

The new model raises the question of how dsDNA is ejected during infection if the channel only allows the dsDNA to travel in one direction. It has been proposed that the motor connector adopts a conformational change after DNA packaging is complete [29]. Such a conformational change renders the channel capable to eject the dsDNA from the viral procapsid. It has been reported that the conformation of the phi29 connector is substantially changed after DNA packaging [29,82,83]. Significant rearrangement of the connector after DNA packaging, a similar feature reported in other phage systems [84–86], may also change the channel configuration to favor the reverse exit of DNA during infection. In bacteriophage p22, a conformational switch of the portal protein primes genome injection [33]. From these results, we confirmed that the connector channel indeed exercises conformational changes. Such conformational changes were induced by molecule binding to the C-terminal wider end that was located within the capsid, and a high electrical voltage shift. The conformational change exhibited three discrete steps, with each step reducing the channel size by 31%.

Our results support the proposal that these three steps of conformational change are regulated by the interaction of DNA with the connector. We demonstrated that the binding or contact of components to the C-terminal would result in the similar discrete steps of conformational change. Conductance assay using mutant connector conjugated with a His-tag to its C-terminal and incubated with anti-His tag antibody or nanogold coated with Ni-NTA revealed three discrete steps of channel change with blockade of about 32% (Fig. 4). It is reasonable to believe that the translocation of DNA into the procapsid or the internal pressure of the fully packaged DNA within the procapsid might lead to the contact of DNA with the C-terminal flexible domain, inducing a conformational change with two subsequent functions: 1) to prevent the dsDNA from exit; and 2) to prepare a new channel configuration to facilitate the injection of DNA during the host cell infection process. The proposed second step of action has also been evidence in the

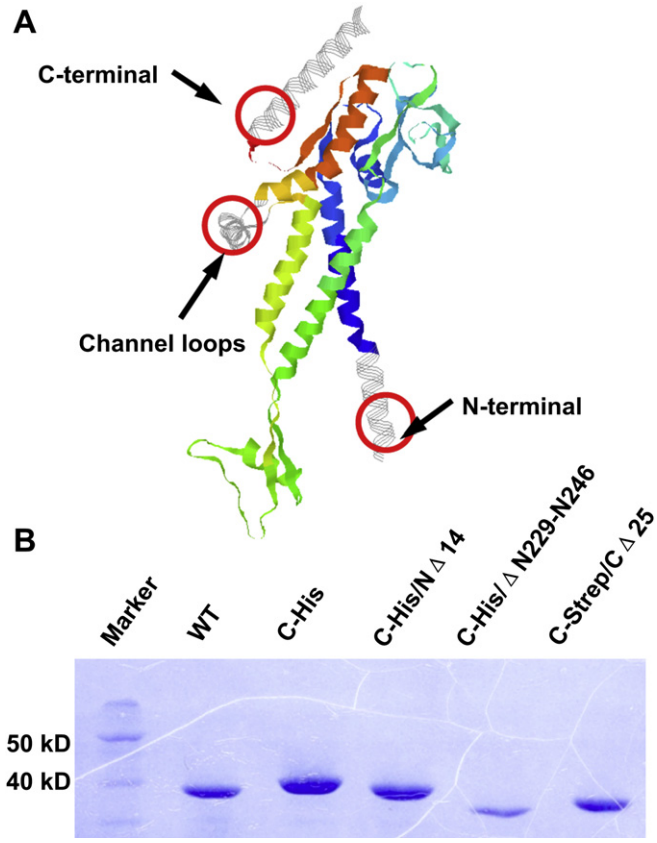

Fig. 5. Rationale for mutant connector design. (A) Structure of one protein subunit of phi29 connector showing the channel loops and the C-terminal [51]; (B) SDS-PAGE of different mutants connectors used in this report.

P22 system [33]. To further support this, a connector mutant with the removal of a 25-amino acid segment at each C-terminal of the 12 subunits were constructed with a strep-tag conjugated to the C-terminal. With this mutant, the discrete steps of 32% conductance change were not observed in the presence of streptavidin. However, conductance assay of the mutant connector by electrical ramping revealed that three discrete steps of conformational changes were also observed (Fig. 6G). The finding suggests that conformational change was a result of the transition of the entire connector structure, and the C-terminal only served as a trigger. This conclusion agrees with the finding in the connector structure of bacteriophage P22 [23]. A unique topology of the C-terminal domain was reported to be a ~200-Å-long α-helical barrel that inserts deeply into the virion and is highly conserved in the Podoviridae family. They proposed that the barrel domain would facilitate genome spooling into the interior of the procapsid during DNA packaging, and in analogy to a rifle barrel to increases the accuracy of DNA ejection during infection. During the course of our investigation, we also found that the batch of the polyclonal antibody made a difference, suggesting that not all binding to any location of the C-terminal would induce a conformational change and certain specific epitope at the C-terminal was important for triggering the conformational change.

The mechanism of ion channel gating has been extensively studied [40]. The ligand-gated ion channels are regulated by a ligand and are usually very selective to one or more ions such as Na^+, K^+, Ca^{2+}, or Cl^-. Such receptors located at synapses convert the chemical signal of a presynaptically released neurotransmitter directly and very quickly into a postsynaptic electrical signal. Conformational changes of α helices in voltage-gated sodium channels and calcium channels have been proposed to explain the gating mechanism. From crystallographic structural studies of the phi29 connector protein, it is possible to surmise that when a potential difference is introduced over the membrane, the associated electromagnetic field induces a conformational change in the protein channel. From the structural viewpoint of a single chain in the connector protein (Fig. 5A), certain areas of the chain are flexible enough to induce a conformational change in response to environmental stimuli. The interaction of dsDNA or phi29 terminal protein gp3 induces a conformational change that distorts the shape of the channel proteins sufficiently such that the cavity, or channel, opens to admit ion influx or efflux across the membrane, down its electrochemical gradient. This conformational change

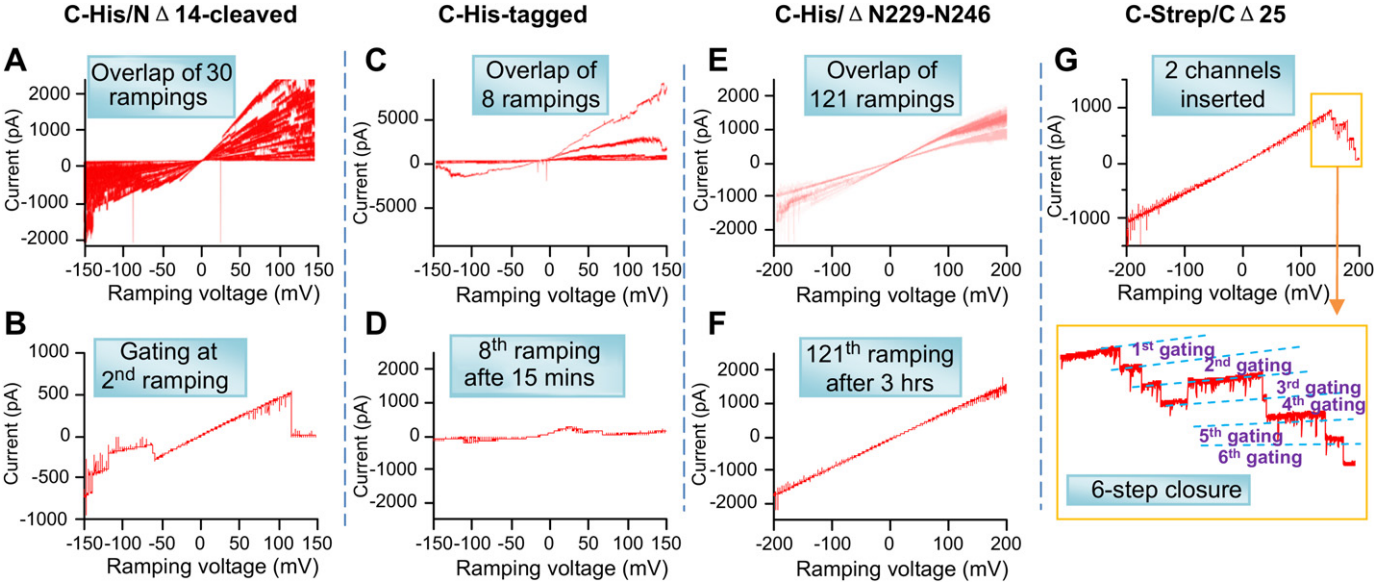

Fig. 6. Summation and superimposition of all current trace collections and comparison between mutants. (A, C, E) Superimposition of multiple current traces under continuous repeated ramping voltages (2.2 mV/s) of individual membrane-connector complexes. (A–B) Representation of gating and reopening of a C-His/NΔ14 connector channel under ramping voltage (−150 mV to +150 mV). The C-His (C–D), the C-His/Δloop (E–F), and the C-Strep/CΔ25 (G) connectors under the ramping voltage were also presented.

leads to the opening or closing of the channel, which help to control the packaging or release of the viral genome.

The controllable opening and closing of the connector protein has been achieved with different polarity, which also resembles the voltage-gated ion channels. However, they have different functions in the biological environment. The ion channels may have to open and close multiple times in their life cycle, whereas the phi29 DNA connector protein might require fewer. The significantly different gating behavior of the internal flexible loop-cleaved connector suggests that the flexible loops may play a key role in the voltage gating. Results described above show that after the removal of these loops, both the occurrence and extent of gating reduced tremendously. These loops can induce conformational changes to adjust the channel size in response to an applied potential. Further studies are necessary to investigate if other domains of the connector protein also contribute to its gating and conformational changes.

5. Conclusions

The real-time direct observation of the viral connector protein opens a new door to study the mechanism of DNA packaging motors. This "modularity" allows us to use these simple and inexpensive model systems to study the regulation of DNA trafficking, the role of the viral portal protein in infection, and pharmaceutical control of the infection. The gating is also reversible and controllable by voltage or ligand binding, making the modified connector protein an ideal nano-valve for constructing nanomachines with potential applications in nanotechnology and nanomedicine, such as for drug loading and controlled release, as well as for high-throughput single pore DNA sequencing.

Acknowledgments

We thank Feng Xiao and Ying Cai for constructing the recombinant connectors, Peng Jing for testing the antibody binding, Randall Reif, Chad Schwartz, Daniel Binzel and Garrett Osswald for assistance in manuscript preparation, and Chris Stites for the preparation of the illustration graphics. The research was supported by GM059944, EB012135 to PG. PG is a co-founder of Kylin Therapeutics, Inc., Viapore, Inc., and Biomotor and RNA Nanotech. Co., Ltd.

References

[1] Guo P. Introduction: principles, perspectives, and potential applications in viral assembly. Semin Virol (Editor's Introduction) 1994;5(1):1–3.
[2] Guo P, Lee TJ. Viral nanomotors for packaging of dsDNA and dsRNA. Mol Microbiol 2007;64:886–903.
[3] Guo P, Peterson C, Anderson D. Prohead and DNA-gp3-dependent ATPase activity of the DNA packaging protein gp16 of bacteriophage phi29. J Mol Biol 1987;197:229–36.
[4] Chemla YR, Aathavan K, Michaelis J, Grimes S, Jardine PJ, Anderson DL, et al. Mechanism of force generation of a viral DNA packaging motor. Cell 2005; 122:683–92.
[5] Hwang Y, Catalano CE, Feiss M. Kinetic and mutational dissection of the two ATPase activities of terminase, the DNA packaging enzyme of bacteriophage lambda. Biochemistry 1996;35:2796–803.
[6] Sabanayagam CR, Oram M, Lakowicz JR, Black LW. Viral DNA packaging studied by fluorescence correlation spectroscopy. Biophys J 2007;93:L17–9.
[7] Meifer WJJ, Horcajadas JA, Salas M. Phi29 family of phages. Microbiol Mol Biol Rev 2001;65:261–87.
[8] Guo P, Erickson S, Anderson D. A small viral RNA is required for *in vitro* packaging of bacteriophage phi29 DNA. Science 1987;236:690–4.
[9] Guo P, Zhang C, Chen C, Trottier M, Garver K. Inter-RNA interaction of phage phi29 pRNA to form a hexameric complex for viral DNA transportation. Mol Cell 1998;2:149–55.
[10] Zhang F, Lemieux S, Wu X, St.-Arnaud S, McMurray CT, Major F, et al. Function of hexameric RNA in packaging of bacteriophage phi29 DNA *in vitro*. Mol Cell 1998;2:141–7.
[11] Moffitt JR, Chemla YR, Aathavan K, Grimes S, Jardine PJ, Anderson DL, et al. Intersubunit coordination in a homomeric ring ATPase. Nature 2009;457: 446–50.
[12] Jimenez J, Santisteban A, Carazo JM, Carrascosa JL. Computer graphic display method for visualizing three-dimensional biological structures. Science 1986; 232:1113–5.
[13] Simpson AA, Leiman PG, Tao Y, He Y, Badasso MO, Jardine PJ, et al. Structure determination of the head-tail connector of bacteriophage phi29. Acta Crystallogr D Biol Crystallogr 2001;57:1260–9.
[14] Guasch A, Pous J, Ibarra B, Gomis-Ruth FX, Valpuesta JM, Sousa N, et al. Detailed architecture of a DNA translocating machine: the high-resolution structure of the bacteriophage phi29 connector particle. J Mol Biol 2002; 315:663–76.
[15] Guo P, Grimes S, Anderson D. A defined system for *in vitro* packaging of DNA-gp3 of the *Bacillus subtilis* bacteriophage phi29. Proc Natl Acad Sci USA 1986; 83:3505–9.
[16] Smith DE, Tans SJ, Smith SB, Grimes S, Anderson DL, Bustamante C. The bacteriophage phi29 portal motor can package DNA against a large internal force. Nature 2001;413:748–52.
[17] Hess H, Vogel V. Molecular shuttles based on motor proteins: active transport in synthetic environments. J Biotechnol 2001;82:67–85.
[18] Soong RK, Bachand GD, Neves HP, Olkhovets AG, Craighead HG, Montemagno CD. Powering an inorganic nanodevice with a biomolecular motor. Science 2000;290:1555–8.
[19] Shu D, Zhang H, Jin J, Guo P. Counting of six pRNAs of phi29 DNA-packaging motor with customized single molecule dual-view system. EMBO J 2007;26: 527–37.
[20] Wendell D, Jing P, Geng J, Subramaniam V, Lee TJ, Montemagno C, et al. Translocation of double-stranded DNA through membrane-adapted phi29 motor protein nanopores. Nat Nanotechnol 2009;4:765–72.
[21] Chang C, Zhang H, Shu D, Guo P, Savran C. Bright-field analysis of phi29 DNA packaging motor using a magnetomechanical system. Appl Phys Lett 2008;93: 153902–3.
[22] Valpuesta JM, Fujisawa H, Marco S, Carazo JM, Carrascosa J. Three-dimensional structure of T3 connector purified from overexpressing bacteria. J Mol Biol 1992;224:103–12.
[23] Olia AS, Prevelige PE, Johnson JE, Cingolani G. Three-dimensional structure of a viral genome-delivery portal vertex. Nat Struct Mol Biol 2011;18: 597–603.
[24] Agirrezabala X, Martin-Benito J, Valle M, Gonzalez JM, Valencia A, Valpuesta JM, et al. Structure of the connector of bacteriophage T7 at 8A resolution: structural homologies of a basic component of a DNA translocating machinery. J Mol Biol 2005;347:895–902.
[25] Bazinet C, King J. The DNA translocating vertex of dsDNA bacteriophages. Annu Rev Microbiol 1985;39:109–29.
[26] Badasso MO, Leiman PG, Tao Y, He Y, Ohlendorf DH, Rossmann MG, et al. Purification, crystallization and initial X-ray analysis of the head- tail connector of bacteriophage phi29. Acta Crystallogr D Biol Crystallogr 2000; 56(Pt 9):1187–90.
[27] Dryden K, Wang G, Yeager M, Nibert M, Coombs K, Furlong D, et al. Early steps in reovirus infection are associated with dramatic changes in supramolecular structure and protein conformation: analysis of virions and subviral particles by cryoelectron microscopy and image reconstruction. J Cell Biol 1993;122: 1023–41.
[28] Jardine P, Coombs DH. Capsid expansion follows the initiation of DNA packaging in bacteriophage T4. J Mol Biol 1998;284(3):661–72.
[29] Tang JH, Olson N, Jardine PJ, Girimes S, Anderson DL, Baker TS. DNA poised for release in bacteriophage phi29. Structure 2008;16:935–43.
[30] Ray K, Oram M, Ma J, Black LW. Portal control of viral prohead expansion and DNA packaging. Virology 2009;391:44–50.
[31] Serwer P, Wright ET, Hakala K, Weintraub ST, Su M, Jiang W. DNA packaging-associated hyper-capsid expansion of bacteriophage T3. J Mol Biol 2010;397: 361–74.
[32] Ionel A, Velazquez-Muriel JA, Luque D, Cuervo A, Caston JR, Valpuesta JM, et al. Molecular rearrangements involved in the capsid shell maturation of bacteriophage T7. J Biol Chem 2011;286:234–42.
[33] Zheng H, Olia AS, Gonen M, Andrews S, Cingolani G, Gonen T. A conformational switch in bacteriophage P22 portal protein primes genome injection. Mol Cell 2008;29:376–83.
[34] Kemp P, Garcia LR, Molineux IJ. Changes in bacteriophage T7 virion structure at the initiation of infection. Virology 2005;340:307–17.
[35] Guo P, Erickson S, Xu W, Olson N, Baker TS, Anderson D. Regulation of the phage phi29 prohead shape and size by the portal vertex. Virology 1991;183: 366–73.
[36] Cy Fu, Prevelige J. *in vitro* incorporation of the phage phi29 connector complex. Virology 2009;394:149–53.
[37] Jing P, Haque F, Vonderheide A, Montemagno C, Guo P. Robust properties of membrane-embedded connector channel of bacterial virus phi29 DNA packaging motor. Mol Biosyst 2010;6:1844–52.
[38] Jing P, Haque F, Shu D, Montemagno C, Guo P. One-way traffic of a viral motor channel for double-stranded DNA translocation. Nano Lett 2010;10:3620–7.
[39] Alberts B, Johnson A, Lewis J, Raff M, Roberts K, Walter P. Molecular biology of the cell. 4th ed. New York: Garland Science; 2002. pp. 615–650.
[40] Hille B. Ion channels of excitable membranes. 3rd ed. Sunderland, MA: Sinauer Associates; 2001. p1–21.

[41] Agnew WS, Simon RL, Brabson JS, Raftery MA. Purification of the tetrodotoxin-binding component associated with the voltage-sensitive sodium channel from electrophorus electricus electroplax Membranes. Proc Natl Acad Sci USA 1978;75:2606–10.
[42] Dorogi PL, Neumann E. Theoretical implication of liganding reactions in axonal sodium channel gating. Neurochem Int 1980;2:45–51.
[43] Sokabe M, Sachs F, Jing ZQ. Quantitative video microscopy of patch clamped membranes stress, strain, capacitance, and stretch channel activation. Biophys J 1991;59:722–8.
[44] Yameen B, Ali M, Neumann R, Ensinger W, Knoll W, Azzaroni O. Ionic transport through single solid-state nanopores controlled with thermally nano-actuated macromolecular gates. Small 2009;5:1287–91.
[45] Lee S, Zhang Y, White HS, Harrell CC, Martin CR. Electrophoretic capture and detection of nanoparticles at the opening of a membrane pore using scanning electrochemical microscopy. Anal Chem 2004;76:6108–15.
[46] Wanunu M, Meller A. Chemically-modified solid-state nanopores. Nano Lett 2007;7:1580–5.
[47] Hou X, Liu Y, Dong H, Yang F, Li L, Jiang L. A pH-gating ionic transport nanodevice: asymmetric chemical modification of single nanochannels. Adv Mater 2010;22:2440–3.
[48] Hou X, Yang F, Li L, Song Y, Jiang L, Zhu D. A biomimetic asymmetric responsive single nanochannel. J Am Chem Soc 2010;132:11736–42.
[49] Cai Y, Xiao F, Guo P. The effect of N- or C-terminal alterations of the connector of bacteriophage phi29 DNA packaging motor on procapsid assembly, pRNA binding, and DNA packaging. Nanomedicine 2008;4:8–18.
[50] Ibanez C, Garcia JA, Carrascosa JL, Salas M. Overproduction and purification of the connector protein of *Bacillus subtilis* phage phi29. Nucleic Acids Res 1984; 12:2351–65.
[51] Guo Y, Blocker F, Xiao F, Guo P. Construction and 3-D computer modeling of connector arrays with tetragonal to decagonal transition induced by pRNA of phi29 DNA-packaging motor. J Nanosci Nanotechnol 2005;5:856–63.
[52] Robinson MA, Wood JP, Capaldi SA, Baron AJ, Gell C, Smith DA, et al. Affinity of molecular interactions in the bacteriophage phi29 DNA packaging motor. Nucleic Acids Res 2006;34:2698–709.
[53] Wanunu M, Morrison W, Rabin Y, Grosberg AY, Meller A. Electrostatic focusing of unlabelled DNA into nanoscale pores using a salt gradient. Nat Nanotechnol 2010;5:160–5.
[54] Serwer P. A hypothesis for bacteriophage DNA packaging motors. Viruses 2010;2:1821–43.
[55] Oram M, Sabanayagam C, Black LW. Modulation of the packaging reaction of bacteriophage T4 terminase by DNA structure. J Mol Biol 2008;381:61–72.
[56] Serwer P. The source of energy for bacteriophage DNA packaging: an osmotic pump explains the data. Biopolymers 1988;27:165–9.
[57] Fujisawa H, Morita M. Phage DNA packaging. Genes Cells 1997;2:537–45.
[58] Astumian RD. Thermodynamics and kinetics of a Brownian motor. Science 1997;276:917–22.
[59] Hendrix RW. Symmetry mismatch and DNA packaging in large bacteriophages. Proc Natl Acad Sci USA 1978;75:4779–83.
[60] Grimes S, Anderson D. The bacteriophage phi29 packaging proteins supercoil the DNA ends. J Mol Biol 1997;266:901–14.
[61] Chen C, Guo P. Sequential action of six virus-encoded DNA-packaging RNAs during phage phi29 genomic DNA translocation. J Virol 1997;71: 3864–71.
[62] Morita M, Tasaka M, Fujisawa H. Structural and functional domains of the large subunit of the bacteriophage T3 DNA packaging enzyme: importance of the C-terminal region in prohead binding. J Mol Biol 1995;245:635–44.
[63] Yu J, Moffitt J, Hetherington CL, Bustamante C, Oster G. Mechanochemistry of a viral DNA packaging motor. J Mol Biol 2010;400:186–203.
[64] Xiang Y, Morais MC, Battisti AJ, Grimes S, Jardine PJ, Anderson DL, et al. Structural changes of bacteriophage phi29 upon DNA packaging and release. EMBO J 2006;25:5229–39.
[65] Ding F, Lu C, Zhao W, Rajashankar KR, Anderson DL, Jardine PJ, et al. Structure and assembly of the essential RNA ring component of a viral DNA packaging motor. Proc Natl Acad Sci USA 2011;108:7357–62.
[66] Zhao H, Finch CJ, Sequeira RD, Johnson BA, Johnson JE, Casjens SR, et al. Crystal structure of the DNA-recognition component of the bacterial virus Sf6 genome-packaging machine. Proc Natl Acad Sci USA 2010;107:1971–6.
[67] Maluf NK, Gaussier H, Bogner E, Feiss M, Catalano CE. Assembly of bacteriophage lambda terminase into a viral DNA maturation and packaging machine. Biochemistry 2006;45:15259–68.
[68] Xiao F, Zhang H, Guo P. Novel mechanism of hexamer ring assembly in protein/RNA interactions revealed by single molecule imaging. Nucleic Acids Res 2008;36:6620–32.
[69] Lowe J, Ellonen A, Allen MD, Atkinson C, Sherratt DJ, Grainge I. Molecular mechanism of sequence-directed DNA loading and translocation by FtsK. Mol Cell 2008;31:498–509.
[70] Skordalakes E, Berger JM. Structural insights into RNA-dependent ring closure and ATPase activation by the Rho termination factor. Cell 2006;127:553–64.
[71] Matias PM, Gorynia S, Donner P, Carrondo MA. Crystal structure of the human AAA+ protein RuvBL1. J Biol Chem 2006;281:38918–29.
[72] McGeoch AT, Trakselis MA, Laskey RA, Bell SD. Organization of the archaeal MCM complex on DNA and implications for the helicase mechanism. Nat Struct Mol Biol 2005;12:756–62.
[73] Fang Y, Cai Q, Qin PZ. The procapsid binding domain of phi29 packaging RNA has a modular architecture and requires 2'-hydroxyl groups in packaging RNA interaction. Biochemistry 2005;44:9348–58.
[74] Fang Y, Shu D, Xiao F, Guo P, Qin PZ. Modular assembly of chimeric phi29 packaging RNAs that support DNA packaging. Biochem Biophysical Res Commun 2008;372:589–94.
[75] Gu X, Schroeder SJ. Different sequences show similar quaternary interaction stabilities in prohead viral RNA self-assembly. J Biol Chem 2011;286: 14419–26.
[76] Chen C, Sheng S, Shao Z, Guo P. A dimer as a building block in assembling RNA: a hexamer that gears bacterial virus phi29 DNA-translocating machinery. J Biol Chem 2000;275(23):17510–6.
[77] Baumann RG, Mullaney J, Black LW. Portal fusion protein constraints on function in DNA packaging of bacteriophage T4. Mol Microbiol 2006;61:16–32.
[78] Hugel T, Michaelis J, Hetherington CL, Jardine PJ, Grimes S, Walter JM, et al. Experimental test of connector rotation during DNA packaging into bacteriophage phi29 capsids. PLoS Biol 2007;5:558–67.
[79] Ray K, Sabanayagam CR, Lakowicz JR, Black LW. DNA crunching by a viral packaging motor: compression of a procapsid-portal stalled Y-DNA substrate. Virology 2010;398:224–32.
[80] Ray K, Ma J, Oram M, Lakowicz JR, Black LW. Single-molecule and FRET fluorescence correlation spectroscopy analyses of phage DNA packaging: colocalization of packaged phage T4 DNA ends within the capsid. J Mol Biol 2010;395:1102–13.
[81] Turner DH, Sugimoto N, Freier SM. RNA structure prediction. Annu Rev Biophys Chem 1988;17:167–92.
[82] Tao Y, Olson NH, Xu W, Anderson DL, Rossmann MG, Baker TS. Assembly of a tailed bacterial virus and its genome release studied in three dimensions. Cell 1998;95:431–7.
[83] Gonzalez-Huici V, Salas M, Hermoso JM. The push-pull mechanism of bacteriophage phi29 DNA injection. Mol Microbiol 2004;52:529–40.
[84] Kemp P, Gupta M, Molineux IJ. Bacteriophage T7 DNA ejection into cells is initiated by an enzyme-like mechanism. Mol Microbiol 2004;53:1251–65.
[85] Lebedev AA, Krause MH, Isidro AL, Vagin AA, Orlova EV, Turner J, et al. Structural framework for DNA translocation via the viral portal protein. EMBO J 2007;26:1984–94.
[86] Lhuillier S, Gallopin M, Gilquin B, Brasiles S, Lancelot N, Letellier G, et al. Structure of bacteriophage SPP1 head-to-tail connection reveals mechanism for viral DNA gating. Proc Natl Acad Sci USA 2009;106:8507–12.